Structural, optical and electrical properties of copper oxide nanoparticles prepared through microwave assistance

S. M. Sathiya[1], G. S. Okram[2], M. A. Jothi Rajan[1*]

[1]*Department of Physics, Arul Anandar College (Autonomous), Karumathur, Madurai 625 514, India*
[2]*UGC DAE Consortium for Scientific Research, University campus, Khandwa Road, Indore 452001, India*

[*]Corresponding author: Tel: (+91) 9486781206; Fax: (+91) 4549287208; Email: anjellojothi@gmail.com

Received: 03 October 2016, Revised: 07 December 2016 and Accepted: 09 April 2017

DOI: 10.5185/amp.2017/605
www.vbripress.com/amp

Abstract

Microwave assisted co-precipitation method is used to synthesize copper oxide nanoparticles from various concentrations of $CuCl_2.2H_2O$ (0.1 M - 0.5 M) precursors. Both CuO and Cu_2O phases are observed from X-ray diffraction (XRD) pattern and further confirmed from Energy Dispersive X-ray Analysis (EDX) and selected area electron diffraction (SAED) data. The particle size of 43 to 27 nm determined from XRD data using Scherrer formula is in good relation with Scanning Electron Microscopy (SEM) and Transmission Electron Microscopy (TEM) images. The existence of reasonably uniform size and shape is clear from SEM. The band gaps determined from the UV-Visible absorption peaks and vibrational modes observed from Micro-Raman Scattering (MRS) analysis further confirm the presence of CuO and Cu_2O phases. These results are also related to electrical conductivity at low temperatures which illustrate different types of conduction mechanisms. The samples show semiconducting behavior with improved electrical conductivity. Finally, the material is proposed to have applications in designing gas sensors and also in regulating electrical conductivity in drug delivery systems.

Keywords: Co-precipitation, microwave, concentration, absorption, microstructure, stoichiometry, conductivity.

Introduction

Metal, semiconductor or oxide nanoparticles are of particular interest for their mechanical, electrical, magnetic, optical, chemical and other physical properties **[1-3]**. Among these, oxides of transition metals are an important class of semiconductors that have wider applications such as magnetic storage media **[4]**, solar energy transformation **[5]**, electronics **[6]** and catalysis **[7]**. Copper oxide, a semiconductor transition metal oxide with a band gap of 1.2 eV, has attracted greater attention since it is used for photoconductive and photothermal applications **[8]**. An improved understanding of nanoparticles and biological cell interactions leads to the development of new sensing, diagnostic, and treatment capabilities, such as improved targeted drug delivery **[9]**, gene therapy, magnetic resonance imaging (MRI) contrast agents **[10]**, and biological warfare agent detection **[11]**. Nano-sized copper oxide possesses good potential for photo-catalytic **[12]**, and sensing applications **[13].** Also**,** their usage in bio-related fields including fouling control and nano-toxicology **[14]** are being explored. Nanoparticles may or may not exhibit size-related properties that differ significantly from those observed in fine particles or bulk materials **[15, 16]**.

In the past few years, the different morphologies of copper oxide nanoparticles like nanorods **[17]**, nanoleaves **[18]**, nanowires **[19, 20],** nanoribbons **[21]**, nanobelts **[22]**, dumbbell-like **[23]**, urchinlike **[24]**, flower-like **[25]** and plate-like **[26]** nanoarchitectures are developed for numerous practical applications. In this direction, vapour and liquid phase techniques are the two broad methods for preparing size and shape selective nanoparticles. Liquid phase techniques **[27 -36] (Table. 1)** were most widely used due to ease in operation and being a promising one to obtain different size and shape. However, each technique has its own merits and demerits in terms of purity of particles, equipment cost and synthesis time **[37]**.

Table 1. Conventional techniques used for copper oxide synthesis.

S. No	Phase	Preparation method	Ref
1.	CuO, Cu_2O	Wet synthesis	**[27, 28]**
2.	CuO	Sol – gel	**[29]**
3.	CuO	Reflux Condensation	**[30]**
4.	CuO	Solution-Phase	**[31]**
5.	CuO	Microemulsion	**[32]**
6.	CuO, Cu_2O	Hydrothermal Synthesis	**[33, 34]**
7.	CuO	Microwave Irradiation	**[35, 36]**

Microwave-based wet synthesis is a novel technique and an important tool that has several advantages such as rapid volumetric uniform heating, higher reaction rate, reaction selectivity, purity, product yield and energy saving **[38]**. This method has provided a new, efficient, and environmentally benign methodology for the synthesis of various metal oxide nanoparticles of diverse morphologies and sizes. As compared to conventional heating, microwaves cause the uniform distribution of temperature between the surface and the bulk material, thereby enhancing the speedy and uniform formation of copper oxide nanoparticles. The main objective of the present work is to investigate the structural, electrical and optical properties of the prepared copper oxide nanoparticles by changing the concentration of the precursor solution. In this work, we report a simple and novel yet robustroute for the microwave-assisted wet synthesis of copper oxide nanoparticles from various concentrations of copper (II) chloride, in addition to exploring their structural, optical and electrical properties.

Experimental

Materials

All the reagents were of analytical grade and were used without further purification. The solutions were prepared with double distilled water. Copper (II) Chloride dehydrate, $CuCl_2.2H_2O$ (CuCl) (99% purity) and sodium hydroxide [NaOH] (97% purity) used in the experiment were procured from Merck, Mumbai, India.

Synthesis of CuO nanoparticles

Copper oxide nanoparticles were prepared by co-precipitation method using various concentrations of CuCl (0.1 M - 0.5 M) in double distilled water in the presence of NaOH **[39, 40]**. Typically, 0.1 M CuCl was dissolved in 100 ml double distilled water at room temperature using a magnetic stirrer for 1 hr and adding NaOH chunks one by one so that its pH attains a value of 12. Then, the solution was kept in a microwave oven (operated with frequency 2.45 GHz and electrical power 800 W) at 120 °C for 1 hr. This resulted in a black coloured precipitate due to the formation of copper oxide nanoparticles. The nanoparticles were separated by centrifugation and cleaned several times with double distilled water and washed with ethanol to remove the other by-products. Then, the nanoparticles were dried in the microwave oven at 200 °C. They were further annealed at 700 °C for 2 hrs in a muffle furnace and used for characterization.

Characterizations

X'Pert Powder PANalytical X-ray diffractometer was used to study the X-Ray Diffraction (XRD) patterns of the synthesized particles. The scan rates were made in the range of 10-70° (2θ) with a step size of 0.02 ° and a count time of 2 sec/step. Optical properties were examined in the range of 200-1200 nm using a Cary 500 scan model and Varian make UV Vis spectrophotometer. SEM analysis was carried out by ESEM-Quanta 200 FEI-Netherlands and EDX measurements were made by EDS-Genesis. Both SEM and EDX mapping were obtained in a high vacuum mode and with an accelerating potential of 200 kV. Micro Raman spectra were recorded on a Renishaw Invia model UV-VIS-NIR Raman microscope (633 nm He-Ne laser source). The electrical conductivity at different temperatures was studied using standard four probe methods. Transmission Electron Microscopy (TEM) analysis was carried out by a 200 kV Tecnai G^2 20 microscope, equipped with a LaB6 filament and a CCD camera.

Results and discussion

The XRD patterns of the synthesized powders are illustrated in **Fig. 1**. The 2θ values of the samples match well with JCPDS files for Cu_2O and CuO (No. 05-0661, 80–0076), corresponding to cubic and monoclinic crystal systems, respectively. It can be seen that the as prepared sample clearly indicates the presence of two crystalline phase indices, monoclinic cupric oxide (CuO) and cubic cuprous oxides (Cu_2O) **[41, 42]**. The peak positions with 2θ values of 35.4°, 61.4° and 72.3° are respectively indexed as (111), (220) and (311) planes which are in good agreement with those of powder Cu_2O obtained from the JCPDS file no.05-0667, confirming the formation of a crystalline cubic phase of Cu_2O with a cuprite structure. Moreover, the peaks at 32.4°, 35.4°, 38.6°, 46.2°, 48.7°, 53.3°, 58.6°, 61.4°, 65.6°, 66.2°, 67.9°, 72.3° and 75.1° can be assigned to (110), (-111), (111), (-112), (-202), (020), (202), (-113), (022), (-311), (220), (311) and (004) planes respectively. These match with the values of monoclinic phase of CuO with the respective JCPDS card no 80–0076 **[43]** and confirms again the presence of CuO phase.

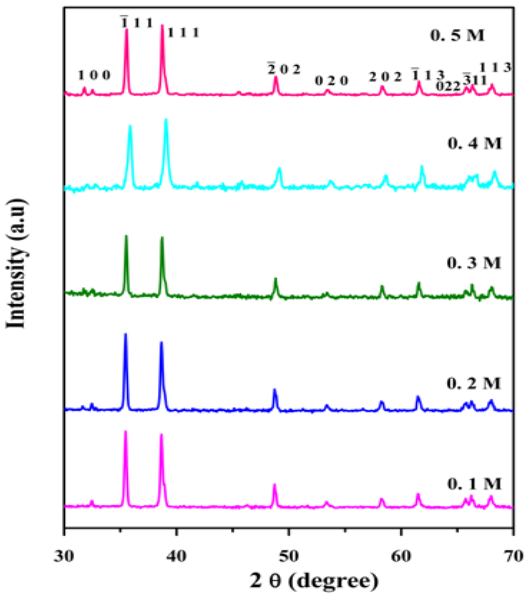

Fig. 1.XRD patterns of copper oxide nanoparticles obtained from 0.1 M to 0.5 M $CuCl_2.2H_2O$.

Table 2. The XRD calculation details of CuO and Cu_2O nanoparticles for 0.1 M to 0.5 M CuCl concentrations.

Mole (M)	Grain size D (nm)		Lattice Strain ε (mm)		Dislocation Density δ x 10^{15} (lines / m^2)		No. of Crystallites N x 10^{20}	
	CuO	Cu_2O	CuO	Cu_2O	CuO	Cu_2O	CuO	Cu_2O
0.1	43	43	0.851	0.819	0.644	0.565	1.797	1.362
0.2	40	43	0.927	0.807	0.775	0.545	2.437	1.284
0.3	40	42	1.048	0.931	1.097	0.818	4.613	2.775
0.4	27	34	1.695	1.149	3.661	1.194	40.48	4.522
0.5	38	41	0.96	0.852	0.818	0.613	2.5675	1.544

Higher intensity at 2θ values of 35.4 ° indicates that the mixed phase has major proportion of CuO with highly oriented crystalline structure. On the basis of diffraction peak intensities, CuO is seemingly the predominant phase. Thus, the amount of cuprous oxide is less than that of cupric oxide **[44]**. This is therefore evidence for the formation of both Cu_2O and CuO nanocrystals in the samples. These results are rather interesting since in earlier studies **[45, 46]**, only CuO phases were proved without performing any measurements to confirm Cu_2O phase. However, in the present study, we performed the UV– visible absorption spectroscopy measurement to clarify the different phase formation.

The relative peak height can be taken as a semi-quantitative measure of the corresponding phase in the nanoparticles **[47]**. The size of the nanoparticles was (with an estimated error of ± 0.5 nm) calculated from the Scherrer's formula which well correlates with that obtained from SEM and TEM studies. The size decreases with increase in CuCl concentration until 0.4 M, beyond which it increases. The grain size (D), lattice strain (ε), dislocation density (δ), number of crystallites (N) of CuO and Cu_2O nanoparticles were calculated and listed in **Table. 2**. Dislocation density value indicates the measure of defects in the structure. A higher dislocation density value indicates lower crystallinity levels of the nanoparticles **[48]**. The XRD calculations show that, when the grain size decreases the lattice strain, dislocation density and the number of crystallites increases up to 0.4 M CuCl but decreases beyond it. Thus, the XRD pattern-derived results prove to be strong evidence in favor of the UV–vis spectra and TEM images for the presence of copper oxide nanoparticles.

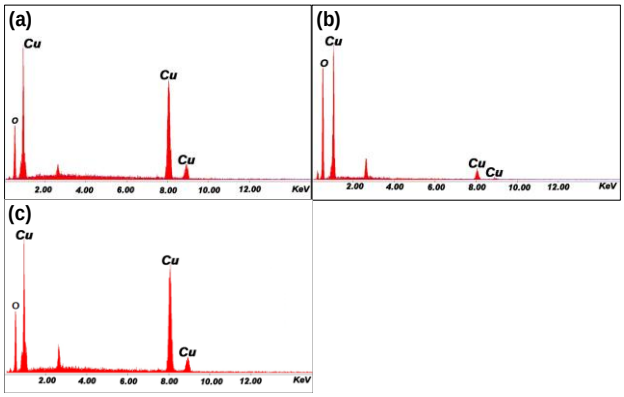

Fig. 2. EDX spectra of copperoxide nanoparticles synthesized from (a) 0.3 M, (b) 0.4 M, and (c) 0.5 M CuCl .

The EDX analysis was performed to investigate the elemental analysis of synthesized materials. As seen in **Fig.2,** the EDX spectrum contains only Cu and O elements without any other elemental impurity. The elemental quantification and stoichiometry ratio of copper oxide nanoparticles were confirmed by X-ray dispersive analysis. Nano copper oxide showed the characterized peak lines around 1.012 and 8.63 keV, which could be attributed to La and Ka for Cu and 0.52 keV for Ka of O, respectively. According to the literature This shows the presence of uniform distribution of particles with copper to oxygen atomic ratio 2:1 and 1:1 in Cu_2O and CuO, respectively, which agrees well with the XRD studies discussed above and also with as the reported results in the literature **[49]**.

Fig. 3 shows the SEM images of the fine copper oxide nanoparticles prepared from 0.3 – 0.5 M precursor concentrations at 700 °C for 2 hrs. It also supports the formation of well-dispersed spherical and regular shaped Cu_2O and CuO nanoparticles, respectively. Due to high surface charge, agglomeration takes place according to Ostwald ripening process. The appearance of the grains is regular and microstructure consists of many neatly arranged spherical shaped particles (nano balls) **[50]**.

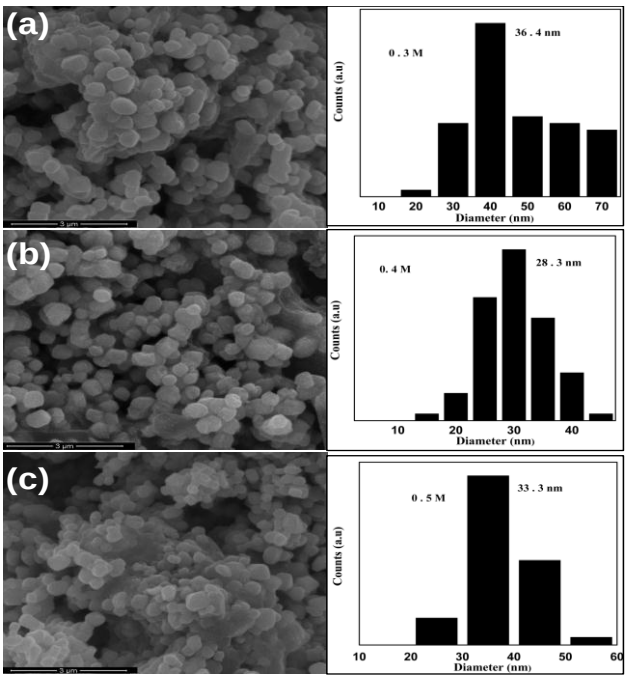

Fig. 3. SEM images and size distribution of copper oxide synthesized from (a) 0.3 M, (b) 0.4 M and (c) 0.5 M (The scale bar is 3 μm).

It is assumed that the polarity of solvent with synthesis technique affects the properties of nanoparticles. The salient features of these powders are that the particles are nearly spherical and their diameters are uniformly distributed. It can also be seen that the given copper oxide nanoparticles having relatively large spherical particles are of uniform size. However, in addition, there were many tiny particles adhering to the bigger spherical particles. The size of the particles decreases **(Table. 3)** with increase in molar concentration up to 0.4 M CuCl but increases beyond it, which is consistent with the information obtained from XRD calculations. When the concentration was increased from 0.3 to 0.5 M, small particles disappear and the relatively large particles became dominant. This shows that the higher concentration results in particle growth in consistent with the literature **[51]**.

Table 3. Crystallite sizes of CuO nanoparticles made from 0.3 M, 0.4 M and 0.5 M precursor concentrations.

Sl . No	Mole (M)	XRD	SEM	TEM
1.	0.3	40	36	40
2.	0.4	27	28	---
3.	0.5	38	33	---

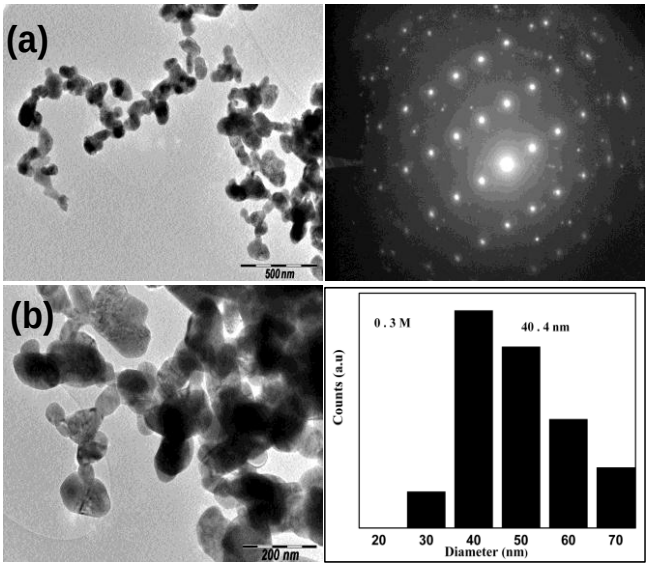

Fig. 4. (a) TEM image, (b) SAED pattern and size distribution of copper oxide nanoparticle (0.3 M).

The TEM images in **Fig. 4 (a)** reveal that the product consists of spherical nanosized particles with a regular morphology and relatively narrow size distribution **[52]**. Majority of the nanoparticles observed from the micrographs are nearly spherical with a small percentage of elongated particles. Moreover, they are quite well dispersed and not agglomerated much with average particle size of 40 nm, which agrees well with XRD results **(Table. 3)**. The presence of diffraction rings in selected area diffraction pattern (SAED) supports the existence of cubic Cu_2O and monoclinic CuO structural phases (**Fig. 4 (b)**) in crystalline form in accordance with the XRD data.

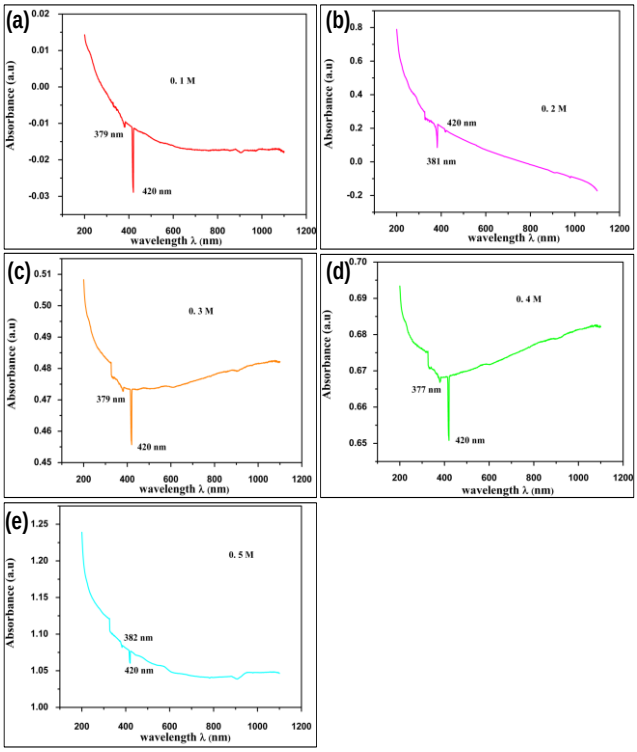

Fig. 5. Absorption spectra of copper oxide nanoparticles prepared at different molar concentrations (a) 0.1 M, (b) 0.2 M, (c) 0.3 M, (d) 0.4 M, (e) 0.5 M.

The absorption spectra in the range 200–1200 nm were recorded for the copper oxide nanoparticles prepared at 700 °C. Peaks at 377 - 382 nm and 420 nm may be attributed to the presence of Cu_2O and CuO, respectively as shown in **Fig. 5[53]**. It also shows that the absorption decreases exponentially with the wavelength and the spectrum is in the visible region. In this absorption spectrum, the lower cut-off region is nearer to 420 nm. When the wavelength of the absorption spectra increases or above the cut-off region the absorption is constant, and here it shows the transparent nature of the copper oxide nanoparticles. The fundamental absorption, which corresponds to electron excitation from the valence band to conduction band, is used to determine the nature and value of the optical band gap. The relation between the absorption coefficients (α) and the incident photon energy (hν) are related by the equation $(\alpha h\nu)^{1/n}=A\ [h\nu - E_g]$, where A is a constant and E_g is the energy band gap of the material and the exponent 'n' depends on the type of transition **[54]**. For directly allowed transitions n=1/2, for indirectly allowed transitions n=2, and for directly forbidden transitions n=3/2. To determine the possible transitions, $(\alpha h\nu)^{1/n}$ versus hν were plotted and the corresponding band gaps were obtained from extrapolation of the straight portion of the graph on 'hν' axis at $\alpha = 0$.

For CuO and Cu_2O nanoparticles, higher direct band gaps were observed compared to their bulk bandgap values. The light absorption creates an electron in the conduction band and a positive hole in the valance band.

The band gap of CuO and Cu_2O nanoparticles increases with increase in molar concentration. The increase in energy gap may be due to the change in concentration of CuCl. The increase in the band gap of the as-prepared copper oxide nanoparticles is indicative of quantum size effects **[55-57]**.

Micro Raman spectroscopy has been widely used to probe the local atomic arrangement and vibrational modes of the nanosized materials **[58]**. Copper oxide belongs to C^6_{2h} group with two molecules per primitive cell. One can find the zone centre Raman Active normal modes Γ_{RA} = 4Au + 5Bu + Ag + 2Bg. There are three acoustic modes (Au + 2Bu), six IR active modes (3Au + 3 Bg), and three Raman active modes (Ag + 2Bg). Three Raman active optical phonons have been identified comparable to the reported data of copperoxide nanoparticles synthesized by other methods **[59]**.

Fig. 6 shows the Raman spectra of the prepared copper oxide nanoparticles. The Raman peaks are broadened; the peak at 224 cm^{-1} can be assigned to be Ag mode for both Cu_2O and CuO, while the peaks at 1317 and 3227 cm^{-1} can be assigned to the Bg modes. Cu_2O phase exhibit only one IR vibrational band in the frequency range of 400–1000 cm^{-1}, due to Cu(I)O vibration. However, CuO phase exhibit three absorption bands corresponding to the vibrations of Cu(II)O bonds in the same frequency range **[60]**. It also shows that the intensity of the spectrum increases with decrease in Raman shift, indicating the decrease in crystallite sizes of copper oxide.

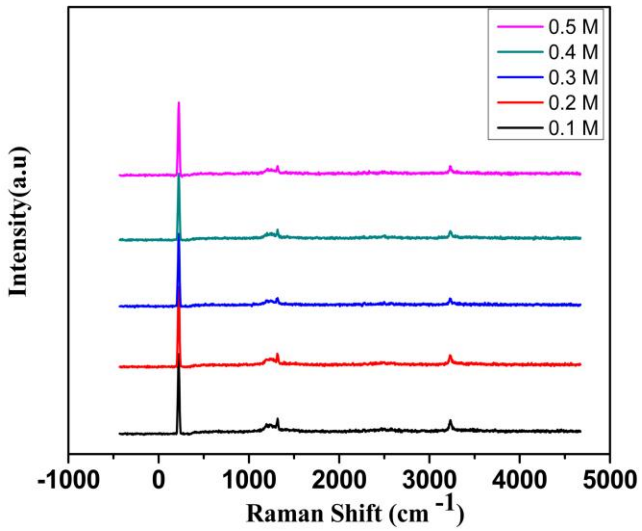

Fig. 6. Micro Raman scattering spectra of copper oxide nanoparticles prepared by co-precipitation method.

In the case of temperature dependence of the semiconductor materials, the conductivity is expressed by the equation: $\sigma=\sigma_o \exp[-E_a/kT]$, where σ_o is the pre-exponential factor E_a is the activation energy for this thermally activated process and k is the Boltzmann constant **[61]**. Clearly a plot of (**Fig. 7**) log (σ) vs. 1000/T will be a straight line up to the moderate temperature. The straight-line nature of the Arrhenius plot indicates the Ohmic conduction, as often found in semiconductors **[62, 63]**.From the plots, it is clear that the conductivity of the nanoparticles is non-linear in general. This resulted in different behaviors of the plots depending on the CuCl concentrations. Up to 0.2 M, the plots have a sharp fall down, however near to 300 K, it increases with increase in temperature indicating the semiconducting behavior of the samples. That is, while the grain size decreases with CuCl concentration, the electrical conductivity drops. The conductivity mechanism in the temperature range studied (100 K-300 K) can be explained using Seto's classical grain boundary effect, which presumes that the conduction process is governed by the thermionic emission over the potential barriers across the grain boundaries.

In the present study, approximately three regions are very distinctly found. The small increase in conductivity at the (region I) low temperature region (190 K – 230 K) could be related either to the competition between CuO and CuO_2 phases or adsorption of oxygen on the surface of the CuO nanoparticles, consistent with literature **[64]**.

In (region II) moderate temperature region (230 – 280 K), the conductivity is not much affected by the temperature change probably due to the equilibrium achieved between the two-competing process of thermal excitation of electrons and oxygen adsorption. Finally, the conductivity in (region III) high temperature region (280 – 300 K) increases with increase in temperature and this is because of the thermal excitation (the process in which atoms or molecules acquire internal energy in collisions with other particles) which is the main cause of increase in electrical conductivity. The concentration of free electrons and holes increases with increasing temperature. Valence electrons take their excitation energy from the lattice by absorbing a phonon. They can be excited at each arbitrary temperature which increases the electrical conductivity of the material.

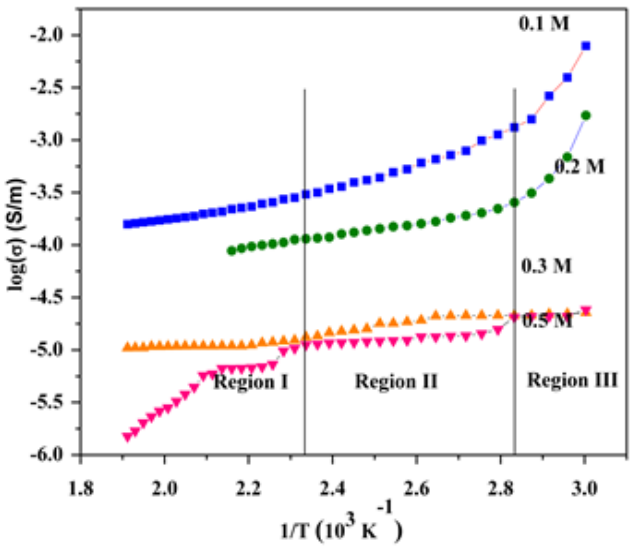

Fig. 7. Variation of log of electrical conductivity σ as a function of inverse of temperature T.

Conclusion

Copper oxide nanoparticles from various precursor concentrations were successfully synthesized using microwave assisted co-precipitation method. The mixed phase nature of CuO and Cu_2O were established in the X-ray diffraction (XRD) and Scanning Electron Microscopy (SEM). The sizes of the grains are regular and microstructure consists of many spherical shaped particles. The particle sizes of the nanoparticles were calculated from XRD data that range from 27 to 43 nm. EDAX results confirm the presence of Cu and O in CuO and Cu_2O compounds. Their vibrational modes were confirmed from the micro-Raman data. Electrical measurements reveal different types of conduction mechanisms in the temperature range 100 K–300 K. The band gaps of CuO and Cu_2O show quantum size effect.

Acknowledgements

The authors (S. M. Sathiya& M. A. JothiRajan) gratefully acknowledge UGC DAE CSR, Indore (India) for financial assistance provided to carry out this work through collaborative research project ref. no. CSR – IC/CRS – 91/2014-15/597.They also are grateful to UGC DAE CSR, Indore Centre (India) for providing XRD and TEM data and Alagappa University, Karaikudi, (India) for micro Raman and UV data.

References

1. Ming-Hui, C.; Hwai-Shen, L.; Clifford Tai, Y; *Powder Technol.***2011**, 207, 378. **DOI:** 10.1016/j.powtec.2010.11.022
2. Abaker, M.; Ahmad, U.; Baskoutas, S.; Kim,S. H.; Hwang, S. W; *J. Phys. D: Appl. Phys.***2011**, 44,155405. **DOI:**10.1088/0022-3727/44/15/155405
3. Chunhua, W.; Yixing, Y.; Bo, T.; Baoyou, G; *Cryst. Eng. Comm.***2012**, 14, 3677. **DOI:** 10.1039/C2CE06707B
4. Rashad, M. M.; Rayan, D. A.; Ramadan, A. A; *J. Mater. Sci.: Mater. Electron.***2013**, 24, 2742. **DOI:**10.1007/s10854-013-1164-8
5. Luwang, M. N; *Appl. Surf. Sci.***2014**, 290, 332. **DOI:**10.1016/j.apsusc.2013.11.077
6. Singh, P. L.; Luwang, M. N.; Srivastava, S. K; *New J. Chem.***2014**, 38, 115. **DOI:**10.1039/C3NJ00759F
7. Stuart, R. T.; Pattanasattayavong, P.; Anthopoulos, T. D; *Chem. Soc. Rev.***2013**, 42, 6910. **DOI:**10.1039/C3CS35402D
8. Javier, V; *J. Phys. Chem. Lett.***2013**, 4, 653. **DOI:**10.1021/jz302100r
9. Dipranjan, L.; Arindam, P.; Sourav, C.; Sandip, K. D.; Somenath, R.; Panchanan, P.; Parimal, K; *RSC Adv.***2015**, 5, 68169. **DOI:** 10.1039/c5ra08110f
10. Perlman, O.; Iris, S. W.; Haim, A; *Phys. Med. Biol.***2015**, 60, 5767. **DOI:**10.1088/0031-9155/60/15/5767
11. Ayekpam, B.; Dinesh, S. M.; Narayan, C. T.; Damayanti, D. M.; Rajen, S. N.; Meitram, N. L; *Chin. Chem. Lett.***2014**, 25, 1615. **DOI:** 10.1016/j.cclet.2014.07.014
12. Zaman, S.; Zainelabdin, A.; Amin, G.; Nur, O.; Willander, M; J. Phys. Chem. Solids, **2012**, 73, 1320. **DOI:**10.1016/j.jpcs.2012.07.005
13. Juan, W.; Wei-De, Z; *Electrochim. Acta*,**2011**, 56, 7510. **DOI:**10.1016/j.electacta.2011.06.102
14. Ren, G.; Hu, D.; Cheng, E. W. C; *Int. J. Antimicrob. Agents*, **2009**, 33, 587. **DOI:** 10.1016/j.ijantimicag.2008.12.004
15. Henrich; Victor; Cox, P. A; *The Surface Science of Metal Oxides*, Cambridge University Press, **2000**. **ISBN:** 0521566878
16. Zhipeng, C.; Jiming, X.; Hui, Z.; Xiaozhong, C.; Juan, S; *Mater. Lett.***2011**, 65, 2047. **DOI:**10.1016/j.matlet.2011.04.021
17. Wang, L.; Gong, H.; Wang, C.; Wang, D.; Tang, K.; Qian, Y; *Nanoscale*, **2012,** 4, 6850. **DOI:**10.1039/c2nr31898a
18. Manoj, D.; Ranjith Kumar, D.; Santhanalakshmi, J; *Appl. Nanosci.***2012**, 2, 223. **DOI:**10.1007/s13204-012-0093-9
19. Anita Sagadevan, E.; Joon Kang, D; *Nanoscale Res. Lett.***2012**, 7, 70. **DOI:**10.1186/1556-276X-7-70
20. Hong, X.; Wang, G.; Zhu, W.; Shen, X.; Wang, Y; *J. Phys. Chem. C*, **2009**, 113, 14172. **DOI:**10.1021/jp9039786
21. Qing, Y.; Hongwen, H.; Ru, C.; Peng, W.; Hangsheng, Y.; Mingxia, G.; Xinsheng, P.; Zhizhen, Y; *Nanoscale*, **2012**, 4, 2613. **DOI:**10.1039/c2nr30135k
22. Reda, M. M.; Farid, A. H.; Ahmed, S; *Ceram. Int.***2014**, 40, 2127. **DOI:** 10.1016/j.ceramint.2013.07.129
23. Wang, H.; Shen, Q.; Xinping, L.; Fenglin, L; *Langmuir*, **2009**, 25, 3152. **DOI:** 10.1021/la803276z
24. Wang, Z.; Xiao, Y.; Xiaobiao, C.; Cheng, P.; Wang, B.; Gao, Y.; Xiaowei, L.; Yang, T.; Zhang, T.; Geyu, L; *ACS Appl. Mater. Interfaces*, **2014**, 6, 3888. **DOI:** 10.1021/am404858z
25. Zhou, B.; Wang, H.; Liu, Z.; Yang, Y.; Huang, X.; Lü, Z.; Sui, Y.; Wenhui, S; *Mater. Chem. Phys.***2011**,126, 847. **DOI:** 10.1016/j.matchemphys.2010.12.030
26. Ling, X.; Hai-Yan, X.; Wang, F.; Feng-Jun, Z.; Ze-Da, M.; Zhao, W.; Won-Chun, O; *J. Korean Ceram. Soc.***2012**, 49, 151. **DOI:**10.4191/kcers.2012.49.2.151
27. Topnania, N.; Kushwaha, S.; Athara, T; *Int.J. Green Nanotechnology: Material Science and Engineering*, **2010**, 1, M67. **DOI:** 10.1080/19430840903430220
28. Yanyan, X.; Dairong,.C.; Xiuling, J.; Keyan, X; *J. Phys. Chem. C*, **2007**, 111, 16284. **DOI:** 10.1021/jp075358x
29. Karthik, K.; Victor Jaya, N.; Kanagaraj, M.; Arumugam, S; *Solid State Commun.***2011**, 151, 564. **DOI:** 10.1016/j.ssc.2011.01.008
30. Bouazizi1, N.; Bargougui, R.; Oueslati, A.; Benslama, R; *Adv. Mater. Lett.***2015**, 6, 158. **DOI:**10.5185/amlett.2015.5656
31. Lijuan, W.; Qing, Z.; Guling, Z.; Yujie, L.; Baoshun, W.; Weiwei, Z.; Bo, L.; Wenzhong, W; Mater. Lett. **2012**, 74, 217. **DOI:** 10.1016/j.matlet.2012.01.123
32. Chengfa, L.; Yin Hou, Y.; Naiying, F.; Yuan, F.; Yanmei, S.; Meng, Q; *Solid State Commun.***2010**, 150, 585. **DOI:** 10.1016/j.ssc.2009.12.039
33. Yunling, Z.; Yan, L.; Zhang, N.; Xiulin , L; *Bull. Mater. Sci.***2011**, 34, 967. **DOI:** 10.1007/S12034-011-0223-0
34. Zheng, Z.; Huang, B.; Wang, Z; Guo, M; Xiaoyan, Q.; Zhang, X.; Wang, P.; Dai, Y; *J. Phys. Chem. C*, **2009**, 113, 14448. **DOI:** 10.1021/jp904198d
35. Min, Y. L.; Wang, T.; Chen, Y. C;*Appl. Surf. Sci.***2010**, 257, 132. **DOI:** 10.1016/j.apsusc.2010.06.049
36. Li, Q. L.; Yong, W; *J. Mater. Chem.***2011**, 21, 17916. **DOI:** 10.1039/C1JM12589C
37. Dar, M. A.; Ahsanulhaq, Q.; Kim, Y. S.; Sohn, J. M.; Kim, W. B.; Shin, H. S; *Appl. Surf. Sci.***2009**, *255*, 6279. **DOI:** 10.1016/j.apsusc.2009.02.002
38. Bilecka, I.; Niederberger, M; *Nanoscale*, **2010**, 2, 1358. **DOI:** 10.1039/B9NR00377K
39. Luna, I. Z.; Hilary, L. N.; Sarwaruddin Chowdhury, A. M.; Gafur, M. A.; Khan, N.; Ruhul Khan, A; *Open Access Library Journal*, **2015**, *2*, e1409. **DOI:** 10.4236/oalib.1101409
40. Tamgadge, Y. S.; Atkare, D. V.; Mahure, M. A.; Gedam, P. P.; Muley, G. G; *JAAST: Material Science*, **2014**, 1, 153.

41. Yu, L.; Xiao-Yu, Y.; Joanna, R.; Guastaaf, V. T.; Bao-Lian, S; *J. Colloid Interface Sci.***2010**, 348, 303. **DOI:**10.1016/j.jcis.2010.04.052
42. Xia, C.; Xiaolan, C.; Ning, W.; Lin, G; *Anal. Chim. Acta.***2011**, 691, 43. **DOI:**10.1016/j.aca.2011.02.037
43. Gao, D.; Zhang, J.; Zhu, J.; Jing, Q.; Zhang, Z.; Wenbo, S.; Huigang, S.; Xue, D; *Nanoscale Res. Lett.***2010**, 5, 769. **DOI:** 10.1007/s11671-010-9555-8
44. Abboud, Y.; Saffaj, T.; Chagraoui, A.; El Bouari, A.; Brouzi, K.; Tanane, O.; Ihssane, B; *Appl. Nanosci.***2014**, 4, 571. **DOI:**10.1007/s13204-013-0233-x
45. Xiang, J. Y.; Tu, J. P.; Huang, X. H.; Yang, Y. Z; *J. Solid State Electrochem*. **2008**, 12, 941. **DOI:**10.1007/s10008-007-0422-1
46. Chen, W.; Chen, J.; Ye-Bin, F.; Hong, L.; Qi-Ying, C.; Ling-Feng, W.; Xin-Hua, L.; Xing-Hua, X; *Analyst*, **2012**, 137, 1706. **DOI:**10.1039/c2an35072f
47. Zhu, H.; Dongxiao, H.; Meng, Z.; Daxiong, W.; Zhang, C; *Nanoscale Res. Lett.***2011**, 6, 181. **DOI:**10.1186/1556-276x-6-181
48. Singh, D. P.; Ojha, A. K.; Srivastava, O. N; *J. Phys. Chem. C*, **2009,** 113, 3409. **DOI:** 10.1021/jp804832g
49. Manimaran, R.; Palaniradja, K.; Alagumurthi, N.; Sendhilnathan, S.; Hussain, J; *Appl. Nanosci.***2014**, 4, 163. **DOI:**10.1007/s13204-012-0184-7
50. Wenzhao, J.; Eliot, R.; Paresh, S.; Edgar, G. R.; Pu-Xian, G.; Yu, L; *Mate. Res. Bull.***2009**, 44, 1681. **DOI:**10.1016/j.materresbull.2009.04.003
51. Wang, W.; Wang, L.; Shi, H.; Liang, Y; *Cryst. Eng. Comm.***2012**, 14, 5914. **DOI:** 10.1039/C2CE25666E
52. Lu, L.; Xirong, H; Microchim. Acta, **2011**, 175,151. **DOI:**10.1007/s00604-011-0663-7
53. Krishnan, S.; Haseeb, A. S. M. A.; Johan, M. R; *J. Alloys Compd.***2014**, 586, 360. **DOI:**10.1016/j.jallcom.2013.10.014
54. **Bhushan,** B.;**Luo,** D.;**Schricker,** S. R.;**Sigmund,** W.;**Zauscher,** S. (Eds.); *Handbook ofNanomaterials Properties*; USA, **2014**. **DOI:**10.1007/978-3-642-31107-9
55. Muslem, F. J.; Raid, A. I.; Khaled, Z. Y; *J. Mater. Sci: Mater. Electron.***2011**, 22, 1244. **DOI:**10.1007/s10854-011-0294-0
56. Hao-Wen, W.; Siang-Yun, L.; Wen-Chung, L.; Kao-Shuo, C; *Appl. Surf. Sci.***2015**, 344, 236. **DOI:** 10.1016/j.apsusc.2015.03.122
57. Tamgadge, Y. S.; Pahurkar, V. G.; Talwatkar, S. S.; Sunatkari, A. L.; Muley, G. G; *Appl. Phys. B*, **2015**, 120,373. **DOI:** 10.1007/s00340-015-6147-4
58. Wenzhong, W.; Qing, Z.; Xiangmin, F.; Yingbo, H.; Pengcheng, Z.; Guling, Z.; Lei, P.; Wenjuan, X; *Cryst. Eng. Comm.***2010**, 12, 2232. **DOI:** 10.1039/B919043K
59. Volanti, D. P.; Keyson, D.; Cavalcante, L. S.; Sim˜oes, A. Z.; Joya, M. R.; Longo, E.; Varela, J. A.; Pizani, P. S.; Souza, A. G; *J. Alloys Compd*.**2008**, 459, 537. **DOI:** 10.1016/j.jallcom.2007.05.023
60. Srivastava, M.; Singh, J.; Rajneesh Mishra, K.; Animesh Ojha, K; *J. Alloys Compd*..**2013**, 555, 123. **DOI:** 10.1016/j.jallcom.2012.12.049
61. Daniel, L. F.; Colby, A. F; *Metal Nanoparticles: Synthesis, Characterization, and Applications*, CRC Press, New York, **2001**. **DOI:**10.1021/ja015381a
62. Rachel, O.; Usha, R.; Sanjeeviraja; *Int. J. Electrochem. Sci*.**2012**, 7, 8288.
63. John, R.; Rajakumari, R; *Nano-Micro Lett.***2012**, 4, 65. **DOI:** 10.3786/nml.v4i2.p65-72
64. Tewari, S.; Bhattacharjee, A; *Pramana–Journal of Physics*, **2011**, 76, 153. **DOI:**10.1007/s12043-011-0021-7

